Journal of Materials Science: Materials in Electronics (2020) 31:4986–4996
https://doi.org/10.1007/s10854-020-03065-8

Judd–Ofelt analysis and physical properties of erbium modified cadmium lithium gadolinium silicate glasses

Kh.S. Shaaban[1] · E. A. Abdel Wahab[2] · A. A. El-Maaref[2,3] · M. Abdelawwad[2,4] · E. R. shaaban[2] · El Sayed Yousef[5,6] · H. Wilke[4] · H. Hillmer[4] · J. Börcsök[4]

Received: 23 December 2019 / Accepted: 7 February 2020 / Published online: 15 February 2020

Abstract
Erbium doped 50SiO_2 -30Li_2O- 1Gd_2O_3- (19 − x) CdO and x Er_2O_3 glass system, where ($0 \leq x \geq 2.5$), mol%, has been prepared by the conventional melt quenching technique. The physical, structural and optical properties are explained by analyzing the data obtained from X-ray diffraction (XRD), Fourier transform infrared (FTIR), UV–Visible (UV–Vis-NIR) and photoluminescence results. X-ray powder diffraction patterns show broad peaks which conform glassy nature of the sample. FTIR spectroscopy reveals the presence of SiO_4, CdO_4 and Er–O vibration groups in the glass samples. The optical absorption spectra in the wavelength range of 200–2500 nm were measured and the optical band gaps, Urbach energy, Electronegativity (χ) Electron Polarizability (α°), and Optical basicity (^) were determined. The optical absorption spectra of Er^{3+} ions in these glasses show eleven bands and are assigned to the transitions from ground state to excited levels. It was found that the optical band gap increases from 3.19 to 3.51 eV with the increase in Er_2O_3 concentration. The strong sharp peak belongs to Er^{+3} emission is investigated in photoluminescence spectra at ordinary condition (1 atm. and at room temperature). It excites by wavelength of 385 nm and gives pale green color at 559 nm. Judd–Ofelt theory has been used to analyze the spectra arising from erbium ions doped 50 SiO_2 -30 Li_2O- 1Gd_2O_3- (19 − x) CdO and x Er_2O_3**.** The intensity parameters $\Omega_{2,4,6}$ of the present complex and lifetimes of selected levels are theoretically calculated as well.

1 Introduction

Glasses doped with rare-earth (RE) ions are important for a wide range of scientific and industrial processes [1]. In the recent decades, extensive research work has been carried out on glasses and glass ceramics doped with rare-earth ions for their use in telecommunication system elements such as upconverters, fibers, optical amplifiers, solid-state lasers and 3D displays. In the last years, many researchers have been investigating different host glasses and glass ceramics doped with rare-earth ions and used it in different applications [2–9]. The application of rare-earth ions doped glasses for laser filed depends on the refractive index of the host materials, bonding of rare-earth ions and the energy of the emitted radiation [2–7]. When the host glass changed, the effect of the rare-earth ions is also changed. This is due to the change in the absorption and radiative properties; this effect can be studied using the Judd–Ofelt theory [8, 9]. In this respect, Er^{3+} ions are the most significant active ions due to their sole energy level structure which have the capability to deliver concurrent green, red emission along with mid IR emission (1530 nm) through both the up and down conversion optical processes.

This is due to the Er^{3+} ion transition around 1.5 μm, which is an eye-safe wavelength. Er-doped silicate, borosilicate, phosphate, and tellurite glasses exhibit superior spectral and laser properties [10–17]. Extraordinarily, Erbium ions doped glass or ceramic glass is more charming due to

✉ Kh.S. Shaaban
khamies1078@yahoo.com

1 Chemistry Department, Faculty of Science, Al-Azhar University, P.O. 71452, Assiut, Egypt

2 Department of Physics, Faculty of Science, Al-Azhar University, P.O. 71452, Assiut, Egypt

3 Physics Department, College of Science, Jouf University, P.O. Box 2014, Skaka, Saudi Arabia

4 Faculty of Electrical Engineering and Computer Science, University of Kassel, Kassel, Germany

5 Physics Department, Faculty of Science, King Khalid University, P.O. Box 9004, Abha, Saudi Arabia

6 Research Center for Advanced Materials Science (RCAMS), King Khalid University, P.O. Box 9004, Abha 61413, Saudi Arabia

the band located at 1550 nm in the infrared region transition between ($^4I_{13/2}$ to $^4I_{15/2}$). erbium doped glasses have numerous applications like microchip lasers [18, 19], amplifier in wavelength division multiplexing systems [18, 20], waveguide amplifiers [21] high-density optical storage and lidar transmitters [22–26]. Silicate glasses have many benefits, based on the availability of designing new types that are suitable for developing up-conversion waveguide laser [27]. The main purpose of this investigation is the preparation of cadmium lithium silicate host glass doped with gadolinium and erbium ions and to investigate its structure and optical properties.

2 Experimental procedures

The $50SiO_2$ -$30Li_2O$- $1Gd_2O_3$- $(19-x)$CdO and x Er_2O_3; where $(0 \leq x \geq 2.5)$, mol% glasses have been synthesized by conventional melting—quenching technique. Pure SiO_2, Li_2O, Gd_2O_3, CdO and Er_2O_3 at a purity of 99.9%, were ground to obtain a mixture for each of the glass samples. The powders produced were then melted in an electrically heated furnace at about 1473 K in regular atmospheric pressure in Pt crucibles, for 4 h to homogenize the melt, which was then added to a preheated mold. This mold was moved right away to a different furnace heated to 673 k for two hours to anneal the glass. Table 1 presents the starting mixtures, also known as nominal composition. The prepared samples' thickness was 0.2 cm, and each was polished in accordance with its use to optical properties. The optical measurements have been studied using a UV spectrometer (JASCO 670).The states of the obtained glasses were identified by X-ray diffractometer. FTIR spectroscopy of the prepared glass samples has been studied at room temperature with the range 400–4000 cm^{-1} by spectrometer type JASCO 430. The experiential setup for measuring the emission spectra consists of a diode-pumped CW laser with emission wavelength of 355 nm as a pumping source, laser beam reshaping optics for collimating the laser beam, infinitely corrected objective and a UV–Vis spectrometer. The power of the diode-pumped CW laser is controlled by two means, first through the adjustment of the power of the pumping diode and second through a round variable neutral density filter. The laser beam passes through a 50/50 beam splitter to the sample and a power meter. The pumping laser spot is expanded collimation by a set of plano-concave and plano-convex cylindrical lenses [26].

Table 1 Chemical composition and preparation of glasses

Sample name	Chemical composition (mol, %)				
	SiO_2	Gd_2O_3	Li_2O	Er_2O_3	CdO
G 1	50	1	30	0	19
G 2	50	1	30	0.5	18.5
G 3	50	1	30	1	18
G 4	50	1	30	1.5	17.5
G 5	50	1	30	2	17

3 Results and discussion

3.1 XRD and FTIR analysis

Figure 1 shows that XRD of present prepared glass samples. It is shown that the curves confirm the glassy nature of the prepared glasses, where no distinguished peaks and no sharp lines, were observed.

Once upon a time the studies of IR spectroscopy on silicate glasses containing alkali have exposed that the glasses structure have not depend on the alkali oxide content and the rule retains the tetravalent valence for the silicon ion [28, 29]. The FTIR spectra of studied glasses are shown in Fig. 2 in the range of 4000–400 cm^{-1}. FTIR spectra give more details about the main groups of the studied glass samples. The basic bands of these glasses are associated to the overlapping of some mono bands with each other. The separated peak has center (C) and its relative area (A). The center of the band is correlated to the vibrations of a specific structural group, while the area under peak is related to the content of these groups as listed in Table 2. Table 3 listed attribution of deconvoluted IR absorption peaks of studied glasses. The values of these parameters agreed well with previous work [30–32]. Figures 3, 4 and 5 presented the deconvoluted spectrum of the glass sample G1, G3& G5. The main absorption band of the studied glasses is identified as follows: [33–45] band at 464–494 cm^{-1} is associated to Cd–O stretching vibration and band at 494 cm^{-1} associated

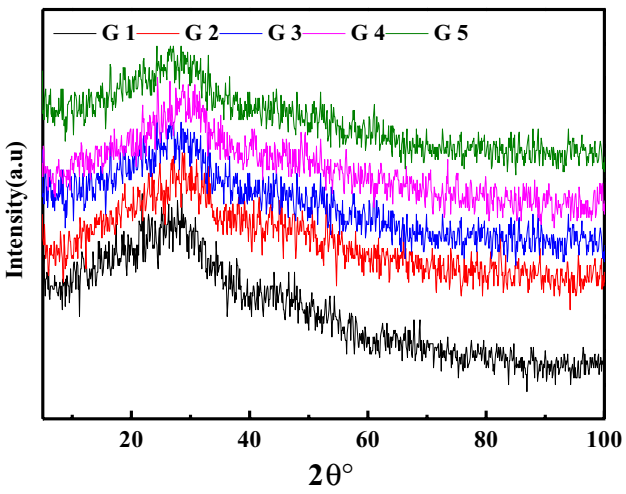

Fig. 1 XRD of the studied glasses

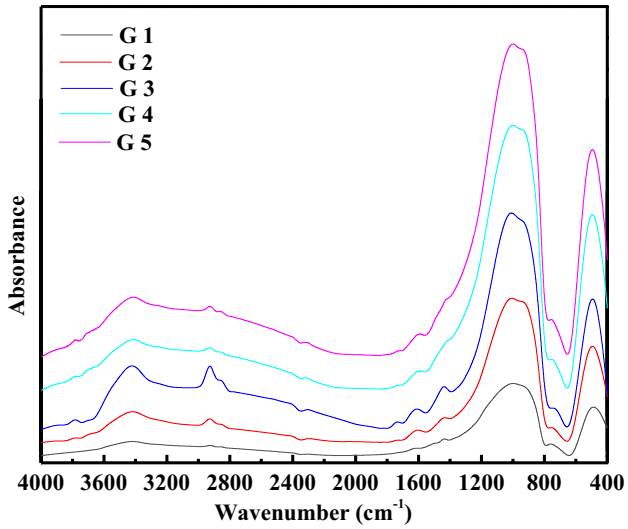

Fig. 2 Infrared spectra of the investigated glasses

to the Er–O vibration. Band at range 400–600 cm^{-1} is generally correlated with Si–O–Si and O–Si–O bending modes of bridging oxygen in the glass network. Band around 524 cm^{-1} is ascribed to the vibrations of the Si–O–Si and O–Si–O bending modes of bridging oxygen and Er–O vibration in the glass network. Band at 600–800 cm^{-1}, the concentration of SiO_4 increase due to the increasing of Si–O stretching. Band around 800–1200 cm^{-1} was associated to the vibration of SiO_4 and CdO_4 tetrahedron and at this absorption band of glass samples was shifted to a higher wavenumber with the increasing Er_2O_3 content due to the increases of the degree polymerization of the glasses. Band at 1002–1086 cm^{-1} is associated to Si–O–Si anti-symmetric stretch of bridging oxygen atoms between tetrahedra, Si–O–Cd anti-symmetric stretching of bridging oxygen within the tetrahedral and Cd–O stretch in CdO_4 units. From Table 2 it can be observed that the band position shifted to higher wavenumber with the increasing Er_2O_3 concentration. This shifting led to change the composition of the glass network due to the addition of Er_2O_3 to glass network.

3.2 Various physical parameters

3.2.1 The erbium ion concentration (Er^{3+})

The ion concentration of Er can be calculated according to the following equation:

$$E_r = \left(\frac{6.023 \times 10\text{^}23x \,\text{mol fraction of cation} \times \text{valency of cation}}{V_m} \right) \quad (1)$$

Table 2 De-convolution parameter of the infrared spectra of studied glasses (C) is the component band center; (A) is the relative area (%) of the component band of the prepared sample

G 1	C	494	–	759	885	–	1002	1203	1333	–
	A	17.6	–	4.68	25.5	–	27.9	17.3	7.05	–
G 2	C	483	–	728	887	–	1005	1153	–	1449
	A	16.6	–	2.41	26.6	–	30.9	18.8	–	4.72
G 3	C	469	524	748	846	956	1077	1269	–	1421
	A	13.3	13.3	2.4	15.7	22.6	20.5	7.71	–	4.42
G 4	C	466	522	737	846	966	1086	1238	–	1435
	A	13.3	13.9	2.33	15.2	23.3	19.8	8.67	–	3.54
G 5	C	464	526	739	855	979	1086	1276	–	1449
	A	13.2	14.1	2.24	16.9	23.3	20	7.06	–	3.25

Table 3 Attribution of deconvoluted IR absorption peaks of studied glasses

Wavenumber (cm^{-1})	Assignment
464–494	Cd–O and Er–O stretching vibration
400–526	Si–O–Si and O–Si–O bending modes
728–759	Cd–O–Cd stretching mode overlapping with Li–O–Si bending vibration
956–979	Si–O–Si stretching of non-bridging oxygen atoms
1002–1086	Si–O–Si anti-symmetric stretch of bridging oxygen atoms between tetrahedra, Si–O–Cd anti-symmetric stretching of bridging oxygen within the tetrahedral and Cd–O stretch in CdO_4 units
1203–1333	O–Si–O stretching vibration of non-bridging oxygen atoms
1421–1449	Shoulder of Carbonate group
2920	Stretching vibrations of [OH] and molecular water

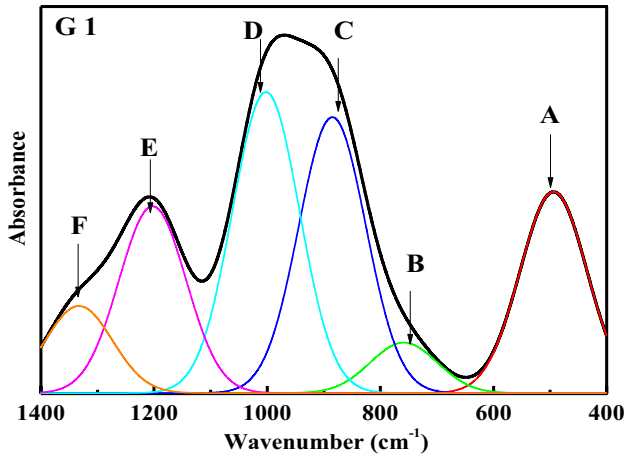

Fig. 3 Curve-fitting of IR spectra of the glass sample G 1

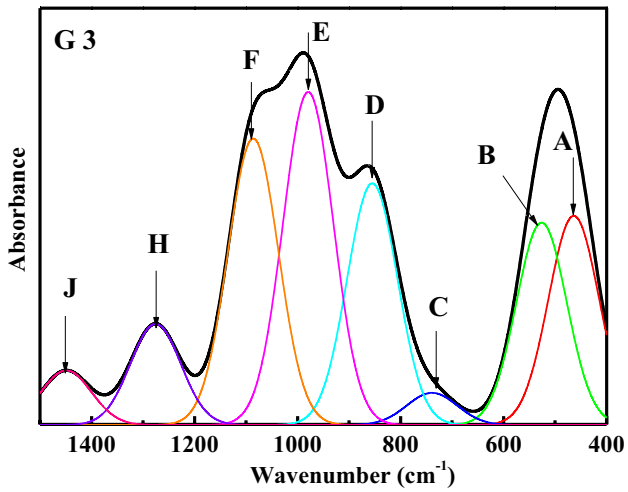

Fig. 4 Curve-fitting of IR spectra of the glass sample G3

The ion concentration of Er values according to Table 4 increased with increase the concentration of erbium. This increase is related to the decrease in the molar volume.

3.2.2 Inter ionic distance (R_i)

The inter ionic distance can be calculated according to the following equation:

$$R_i = \left(\frac{1}{Er}\right)^{\frac{1}{3}} \tag{2}$$

The inter ionic distance between two ions is used to give knowledge about the bond length. The values of R_i according to Table 4 decrease as the content of erbium increases. This decrease is connected to the molar volume.

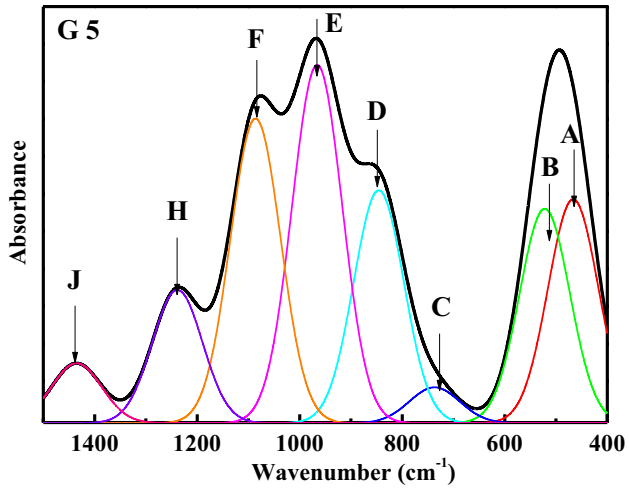

Fig. 5 Curve-fitting of IR spectra of the glass sample G5

The molar refractivity (R_m), molar polarizability (α_m) and Reflection loss (R_L) of the samples can be calculated using these relations:

$$R_m = V_m\left(1 - \sqrt{E_g/20}\right) \tag{3}$$

$$\propto_m = \left(\frac{3}{4\pi N}\right)R_m \tag{4}$$

$$R_L = \left(\frac{R_m}{V_m}\right) \tag{5}$$

The molar refractivity (R_m) depends on the molar polarizability (α_m) of the material. It was found that from (Table 4) the values of (R_m), (α_m) and (R_L) are decreased with increasing the erbium content. The decrease in these values is related to molar volume, formation of bridging oxygen BO, and the decreasing number of free electrons.

The metallization criterion can be estimated by:

$$M = 1 - \frac{R_m}{V_m} \tag{6}$$

The metallization of the prepared samples is shown in Table 4. It was found that metallization decreases with increasing the erbium concentration, which related to a decrease in the Reflection loss (R_L).

The optical electronegativity (χ) of the prepared samples can be calculated from the following relation:

$$\chi = 0.2688E_g \tag{7}$$

where E_g is the optical band gab. So, the electronegativity (χ) increase with increasing of erbium concentration.

Table 4 Various physical parameters of the studied glasses

Samples	G 1	G 2	G 3	G 4	G 5
Number of oxygen atom	1.52	1.53	1.54	1.55	1.56
Avg. Mol. Wt. M_w (mol)	67.23	68.4	69.57	70.74	71.91
Density ρ (gm/cm^3)	3.12	3.19	3.27	3.43	3.51
Molar Volume V_m (cm^3/mol)	21.5	21.4	21.3	20.6	20.5
Ion conc. (N_i) (10^{20} ions/cm^3)	0	4.22	8.51	13.2	17.7
Inter ionic distance Ri (A°)	0	13.54	10.73	9.27	8.41
Oxygen packing density (O_{PD}) (g-atom/l)	70.54	71.36	72.39	75.16	76.15
Urbach energy (E_u) (eV)	0.353	0.314	0.25	0.266	0.227
Indirect band gap energy E_g (eV) [$n=2$]	3.19	3.24	3.42	3.5	3.51
Molar Refractivity R_m (cm^3/mol)	12.94	12.81	12.48	12.00	11.9
Molar polarizability α_m (A$^{\circ 3}$)	5.13	5.08	4.95	4.76	4.72
Metallization criterion (M)	0.399	0.403	0.413	0.418	0.419
Reflection loss (R_L)	0.601	0.597	0.587	0.582	0.581
Electronegativity (χ)	0.857	0.871	0.919	0.941	0.943
Electron polarizability (α°)	2.73	2.72	2.67	2.65	2.65
Optical basicity (^)	1.6297	1.630	1.6302	1.6305	1.6307

Electronic polarizability and optical basicity of the prepared samples are estimated from the following relations:

$$\alpha^{\circ} = -0.9\chi + 3.5 \tag{8}$$

$$\wedge = -0.5\chi + 1.7 \tag{9}$$

Electronic polarizability and optical basicity have the opposite trend value of electronegativity (χ); so, the electronic polarizability and optical basicity values are decreasing with increasing the concentration value of erbium. The decrease in optical basicity value of these glasses is due to that the basicity value of CdO (1.1) is higher than the basicity of erbium (0.929) [46–50].

3.3 Optical characterization

The absorption spectrum in the range of 200–2700 nm of prepared glass has been measured by the UV Jasco 670 and present in Fig. 6. It is observed that, several peaks in the range of 300–1600 nm, due to effect of $f \rightarrow f$ orbital from the Er ions transition. Figure 7 shows the relation between the absorbance coefficient of the prepared samples versus the wavelength. The optical energy gap of the present glass has been estimated by Tauc's formula [49, 50].

$$\alpha.h\nu = C(h\nu - E_g)^k \tag{10}$$

where E_g is the optical band gap, C is an energy independent constant, and the exponent k takes different values ($k=2$ for non-direct transitions). The intercept of $\sqrt{\alpha h\nu}$ versus hν at $\sqrt{\alpha h\nu} = 0$ denoted the value of $E_g$as shown in Fig. 8. The most obvious finding to emerge from the analysis is that the

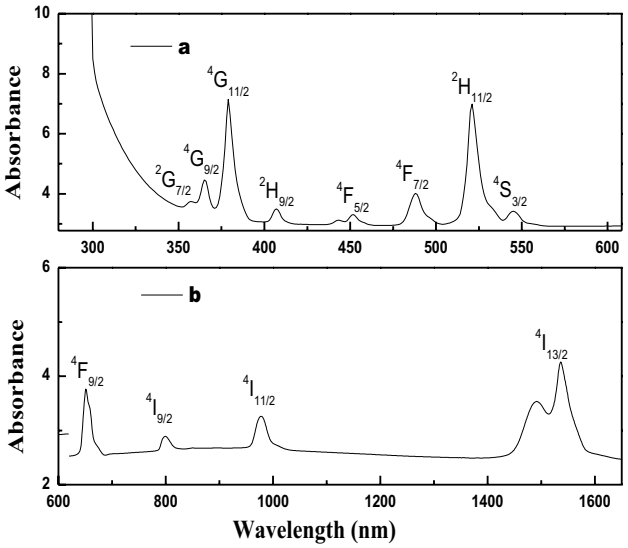

Fig. 6 Absorbance of glass system **a** versus wavelength range of 250–620 nm, **b** from 600 to 1650 nm

energy band gap increases with increase the erbium content and tabulated in Table 4. The increasing of energy gap associated to the increase of localized states and formation of bridge oxygen. The increase of bridging oxygen causes a decrease in the number of donor center leads to increase of the optical band gap [51–56].

The values of Urbach energy have been estimated from the slope of the graph between ln(α) versus the photon energy as shown in Fig. 9 and the values in Table 4. It is observed that decreasing of E_u by increasing the erbium ions content in the samples. Figure 10 shows the relation between E_g and E_u versus the Er content in the samples.

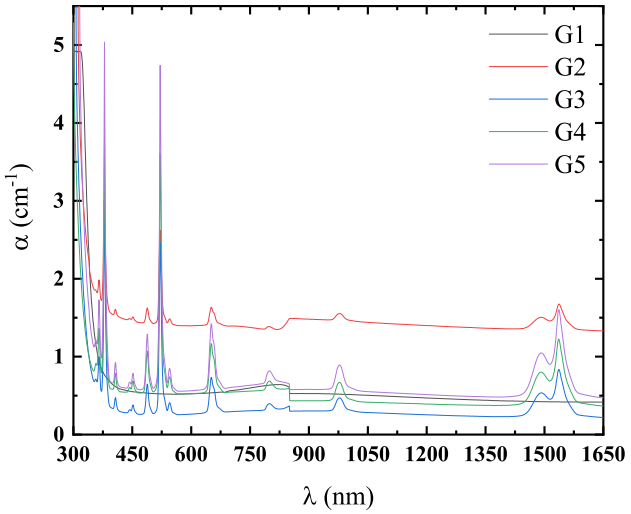

Fig. 7 Optical absorption coefficient of glass system

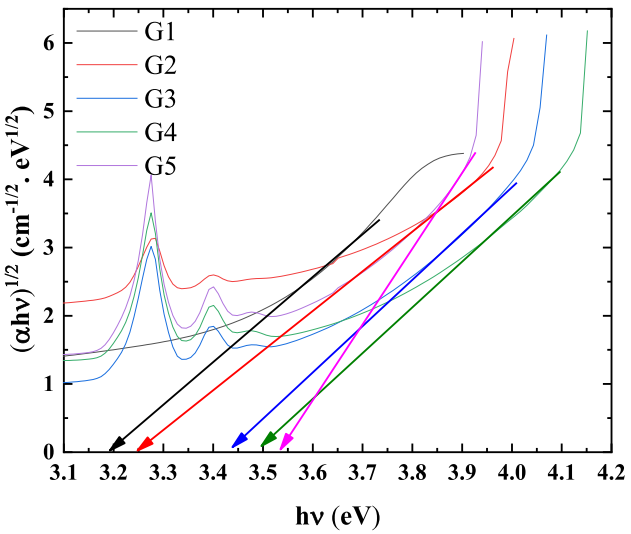

Fig. 8 Plot of $(\alpha\ h\nu)^{1/2}$ against photon energy (hν) to calculate the optical band gap from the intercept of the curves

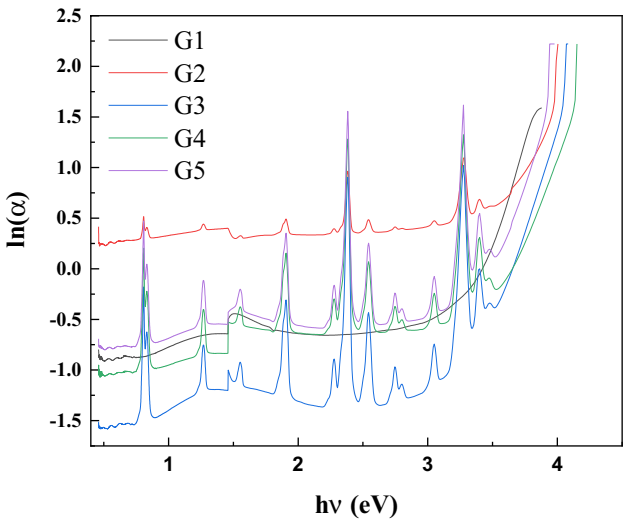

Fig. 9 Plot of ln(α) versus the photon energy (to estimate the Urbach energy from the slope of the liner range of the curves)

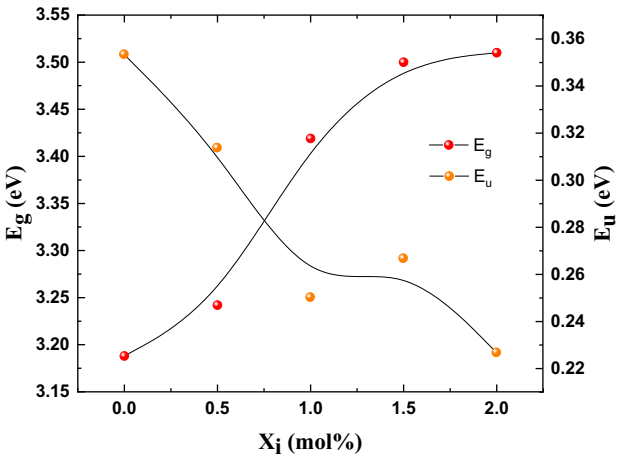

Fig. 10 Optical band gap and Urbach energy versus concentration of Er

It clear that from the figure E_g have direct proportional with the Er content and E_u have inverse proportional with Er content. The increasing values of E_g by increasing the Er_2O_3 content can be understood in terms of the structural changes that are taking place in the prepared glasses caused by the addition of Er_2O_3. This consequence suggests that Er_2O_3 enters into the glass system and it modifies the glass network in such a way that more number of BOs created thus leads to increasing band gap values. Therefore, as discussed previously, increasing the Er_2O_3 content decreases the bond length of the structural units, which in turn is in direct proportionality to the molar volume, and also creates more BOs. These factors, besides the density of Er_2O_3 (8640 kg m^{-3}) is higher than the density of CdO (8150 kg m^{-3}) and bond dissociation energies of Er–O (611 kJ mol^{-1}) is higher than the bond dissociation energies of Cd–O (142 kJ mol^{-1}), are responsible for the increase of E_g values. Urbach energy E_u value decreased with increasing Er_2O_3 content. This may indicate that the addition of Er_2O_3 decreases the disorder of glass systems. Also the oxygen packing density of the prepared glasses gives a good information on their structure. Otherwise the value of oxygen packing density increases with increasing Er^{3+} concentration. This indicates that the glass matrix gets more compact. The presence of erbium ion increases the formation of bridging oxygen ions which result the decreasing number of free electrons in the glass system.

This will result in the increasing value of optical band gap as the concentration of erbium increases [57–61] (Table 4).

The molar refractivity and molar polarizability are decreased with the increase of Er content in the glass as well as the Reflection loss (R_L) and Electron Polarizability (α°) are decreased. On the other hand, metallization criterion (M), Electronegativity (χ) and Optical basicity (ˆ) are increased by increasing Er content as shown in Table 4. The emission spectrum as a result of excitation with a 355 nm CW laser is shown in Fig. 11 where several emission transitions are observed i.e., 423 nm, 458 nm, 523 nm, 533 nm, 547 nm, 558 nm and 732 nm. The maximum two transitions are at wavelength of 547 nm and 558 nm. The emission spectrum is used to calculate the chromaticity coordinates according to the Commission international de l'clairage (CIE 1931) as shown in Fig. 12 [62]. Er^{3+} doped $50SiO_2$ -$30Li2O$- $1Gd_2O_3$- $(19-x)$ CdO has *x* chromaticity coordinate of 0.29 and y chromaticity coordinate of 0.51. That means, the emission of the proposed compound lays in the green emission region.

3.4 Judd–Ofelt analysis

Judd–Ofelt theory [8, 9] has been used to analyze the spectra arising from $4f^n$-$4f^n$ transitions of erbium ions doped $50SiO_2$ -$30Li_2O$- $1Gd_2O_3$- $(19-x)$ CdO. In the present work, the optical parameters such as radiative rates, intensity parameters and line strengths for transitions from ground state to excited states of Er^{3+} hosted by $50SiO_2$ -$30Li_2O$-$1Gd_2O_3$- $(19-x)$ CdO, have been calculated. Most of *f–f* transitions are electronic dipole (ED) transitions and the minority are magnetic dipole (MD) transitions. To calculate line strengths and radiative rates, the reduced matrix operator $U^{(t)}$ applied to the wave functions of upper and

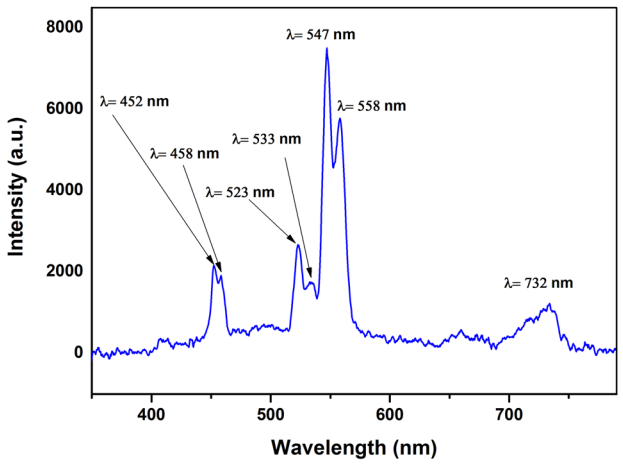

Fig. 11 Emission spectrum of Er^{3+} doped $50SiO_2$ -$30Li_2O$- $1Gd_2O_3$- $(19-x)$ CdO

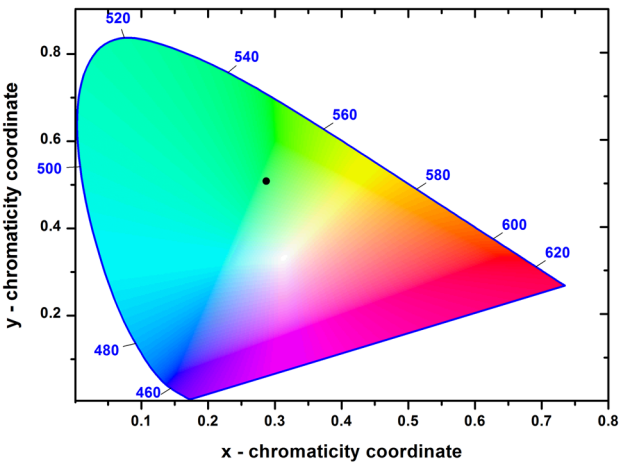

Fig. 12 Chromaticity coordinates calculated from the emission spectrum of Er^{3+} doped $50SiO_2$ -$30Li_2O$- $1Gd_2O_3$- $(19-x)$ CdO

lower states, which available for the $4f^n$ states. The electronic dipole line strength can be calculated form:

$$S_{ED}(J,J') = \sum_{t=2,4,6} \Omega_t \left| f^n[LS]JU^{(t)}f^n[L'S']J' \right|^2 \quad (11)$$

The intensity parameters $\Omega_{t=2,4,6}$ can be determined experimentally from the absorption spectra. New values reduced matrix elements, $U^{(t)}$, of Er^{3+} are listed in Table 5. The experimental line strength S_m is determined from absorption cross-section over the wavelength range of number of transitions by:

$$S_m = \frac{3ch(2J+1)}{8\pi^3 e^2 \overline{\lambda}} n\left(\frac{3}{n^2+2}\right)^2 \int \sigma(\lambda)d\lambda \quad (12)$$

where *J* is the total angular momentum of the lower level, $J = L \pm S$, λ is the mean wavelength of the peak, and

Table 5 Reduced matrix elements

Manifold	U^2	U^4	U^6
$^2G_{7/2}$	0.0000	0.0174	0.0163
$^4G_{9/2}$	0.0000	0.1415	0.0234
$^4G_{11/2}$	0.8184	0.1261	0.0002
$^4F_{3/2}$	0.0000	0.0000	0.3072
$^4F_{7/2}$	0.0000	0.2469	0.7265
$^2H_{11/2}$	0.7126	0.4124	0.0925
$^4S_{3/2}$	0.0000	0.0000	0.5011
$^4F_{9/2}$	0.0000	0.5354	0.4618
$^4I_{9/2}$	0.0000	0.1093	0.0099
$^4I_{11/2}$	0.0282	0.0593	0.9953
$^4I_{13/2}$	0.0195	0.1173	1.4316

the integral of absorption cross-section over wavelength $\int \sigma(\lambda)d\lambda$ is the integration of cross-section as a function of wavelength.

Figure 6a, b depcits UV–Vis-NIR spectra of the investigated glasses in the wavelength region 250–1800 nm. The band positions have been identified at wavelengths of 357, 365, 378, 451, 488, 521, 544, 650, 800, 978, and 1537 nm. These bands are corresponding to transitions in Er^{3+} ion from the ground state $^4I_{15/2}$ to excited levels have the atomic terms ($^{2S+1}L_J$) $^2G_{7/2}$, $^4G_{9/2}$, $^4G_{11/2}$, $^4F_{3/2}$, $^4F_{7/2}$, $^2H_{11/2,}$ $^4S_{3/2}$, $^4F_{9/2}$, $^4I_{9/2}$, $^4I_{11/2}$ and $^4I_{13/2}$, respectively.

J–O calculations of experimental and theoretical line strengths of ground-excited transitions of $^2G_{7/2}$, $^4G_{9/2}$, $^4G_{11/2}$, $^4F_{3/2}$, $^4F_{7/2}$, $^2H_{11/2,}$ $^4S_{3/2}$, $^4F_{9/2}$, $^4I_{9/2}$, $^4I_{11/2}$ and $^4I_{13/2}$ glasses doped with different concentrations of Er_2O_3 are listed in Table 6. It is observed that the strong intensities are recorded at $^4G_{11/2}$ and $^2H_{11/2}$ transitions with wavelength of 378, 521 nm, respectively, which obviously clear in Fig. 6, as well. These transitions have recorded line strengths values of 1.74–8.33 (dimensionless) for $^4G_{11/2}$ and 1.59–9.4 for $^2H_{11/2}$.

In Table 6, for the most measured and calculated values of line strengths there is no certain trend followed. The reasonable agreement between experimental (S_m) and theoretical line strengths (S_{th}) can be assisted from the root mean square deviations (RMS). RMS values are lower in the present work which in the same order for those recorded in other literature [63, 64]. It is obvious that the values of S_m and S_{th} show good agreement for most transitions such as $^4G_{11/2}$, $^4F_{7/2}$, $^2H_{11/2}$ and $^4F_{9/2}$. However, in the cases of weak transitions, a large deviation between S_m and S_{th} has been observed for such as $^2G_{7/2}$ and $^4I_{13/2}$. These big differences may be due to the sensitivity of the line strengths for the choice of the wave functions.

The least squares fit method has been applied over a set of reduced matrix elements and experimental values of spectral intensities to calculate the optical intensity parameters, $\Omega_{t=2,4,6}$. Calculated values of Ω_2, Ω_4, and Ω_6 have been listed in Table 7. As it clear in Table 3, the J-O intensity parameters of the Er^{3+} doped glass decrease with the increasing of Er_2O_3 concentration in the prepared compositions; this might be due to the quenching processes within the compound [63, 64].

The radiative rates (lifetimes and transition probabilities) of Er^{3+} doped $50SiO_2$ -$30Li_2O$- $1Gd_2O_3$- $(19-x)$ CdO are shown in Figs. 13 and 14. Lifetime values of $^4I_{9/2,11/2,13/2}$ as a function of Er_2O_3 content are shown in Fig. 13. It is obviously clear that the lifetime values of the selected levels in Er^{3+} decreased with the increasing of Er_2O_3 content. This trend may be attributed to the quenching processes which dominate the internal processes inside the present composition. As well as, the variation of theoretical spectrum over a wavelength range of about 350–1200 nm is shown in Fig. 14. The largest values of transition probabilities appear at low wavelength rang up to 650 nm. This is because the transition probability depends on the band energy (ΔE) which decreases by increasing of wavelength.

4 Conclusion

The addition of erbium to the cadmium lithium silicate glasses leads to the modification of the glass network resulting higher optical band gap. The FTIR spectra of the present

Table 7 Intensity parameters

Sample	Ω_2	Ω_4	Ω_6
0.5	1.82 ± 0.09	1.02 ± 0.14	0.18 ± 0.04
1.0	8.49 ± 0.31	7.86 ± 0.50	1.25 ± 0.16
2.0	5.40 ± 0.55	3.55 ± 0.88	1.93 ± 0.29
3.0	2.85 ± 0.40	3.29 ± 0.64	1.20 ± 0.21

Table 6 Measured and calculated line strengths (S-values) of Er^{3+} doped glasses at different concentrations

Manifold	λ, nm	E, cm−1	0.5		1.0		2.0		3.0	
			S_m	S_{th}	Sm	Sth	Sm	Sth	Sm	Sth
$^2G_{7/2}$	357	28,011	0.0154	0.0206	0.1221	0.1573	0.1978	0.0933	0.0914	0.0768
$^4G_{9/2}$	365	27,397	0.2433	0.1483	1.4565	1.1421	0.8892	0.5474	0.4300	0.4936
$^4G_{11/2}$	378	26,455	1.7454	1.6213	8.3263	7.9385	5.1662	4.8660	2.5706	2.7485
$^4F_{3/2}$	451	22,172	0.0437	0.0547	0.5252	0.3847	0.4129	0.5946	0.2781	0.3680
$^4F_{7/2}$	488	20,491	0.3860	0.3808	3.1583	2.8508	1.5947	2.2818	1.1211	1.6823
$^2H_{11/2}$	521	19,193	1.5953	1.7363	8.9670	9.4066	5.1459	5.4887	3.7012	3.4988
$^4S_{3/2}$	544	18,382	0.0898	0.0892	0.7895	0.6276	0.7673	0.9700	0.3401	0.6004
$^4F_{9/2}$	650	15,384	0.6835	0.6275	4.8759	4.7875	3.0511	2.7926	2.3348	2.3140
$^4I_{9/2}$	800	12,500	0.0918	0.1130	0.8294	0.8714	0.6357	0.4067	0.5728	0.3712
$^4I_{11/2}$	978	10,224	0.2254	0.2890	2.0002	1.9519	1.6672	2.2889	1.0584	1.4677
$^4I_{13/2}$	1537	6506	0.4433	0.4099	2.5998	2.8808	4.1135	3.2924	2.8161	2.1566
Rms			0.0815		0.2905		0.5076		0.3727	

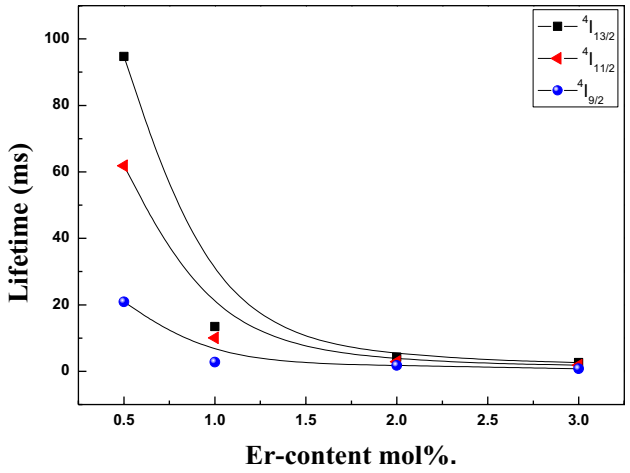

Fig. 13 Lifetime of selected levels in Er ions as a function of RE content

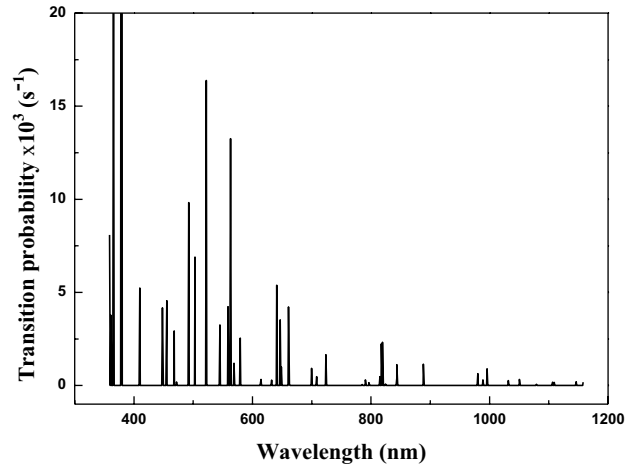

Fig. 14 Theoretical spectrum of Er^{3+} doped $50SiO_2$ -$30Li_2O$-$1Gd_2O_3$- $(19-x)$ CdO

glass system have been deconvoluted and contribution from different glasses modifier have been identified. Moreover, the density increases with the concentration of erbium content and the molar volume decrease, while the molar refractivity, molar polarizability, reflection loss and optical basicity decreased. Judd–Ofelt method has been used to calculate the optical parameters of the prepared glasses doped Er^{3+}. The present calculations of line strengths, optical intensity parameters (Ω_t), and radiative lifetimes show that there is no specific trend in the line strengths with the concentration of rare earths while the intensity parameters and lifetimes decrease with the increasing of Er_2O_3 concentration. This trend is justified to the quenching processes that dominate the internal processes inside the composition. The prepared glasses are excellent candidates for laser applications.

Acknowledgements The authors are grateful to Al-Azhar University for supporting with the experimental measurements. In addition, the authors thank the Deanship of Scientific Research at King Khalid University (KKU) for funding this research project, Number: (R.G.P2./22/40) under research center for advanced material science.

References

1. S.N. Nazrin, M.K. Halimah, F.D. Muhammad, Comparison study of optical properties on erbium-doped and silver doped zinc tellurite glass system for non-linear application. J. Mater. Sci. **30**, 6378 (2019)
2. M.N. Azlan, M.K. Halimah, H.A.A. Sidek, Linear and nonlinear optical properties of erbium doped zinc borotellurite glass system. J. Lumin. **181**, 400–406 (2017)
3. Y. Nageno, H. Takebe, K. Morinaga, Correlation between radiative transition probabilities of Nd^{3+} and composition in silicate, borate, and phosphate glasses. J. Am. Ceram. Soc. **76**, 3081–3086 (1993)
4. A.R. Devi, C.K. Jayasankar, Optical properties of Nd^{3+} ions in lithium borate glasses. Mater. Chem. Phys. **42**, 106–119 (1995)
5. V. Mehta, G. Aka, A.L. Dawar, A. Mansingh, Optical properties and spectroscopic parameters of Nd^{3+} doped phosphate and borate glasses. Opt. Mater. (Amsterdam) **12**, 53–63 (1999)
6. E. Pecoraro, J.A. Sampaio, L.A.O. Nunes, S. Gama, M.L. Baesso, Spectroscopic properties of water free Nd_2O_3-doped low silica calcium aluminosilicate glasses. J. Non Cryst. Solids **277**, 73–81 (2000)
7. E. Snitzer, R. Woodcock, Yb^{3+}–Er^{3+} Glass laser. Appl. Phys. Lett. **6**(3), 45–46 (1965)
8. B. Judd, Optical absorption intensities of rare-earth ions. Phys. Rev. **465**(127), 750–761 (1962)
9. G. Ofelt, Intensities of crystal spectra of rare earth ions. J. Chem. Phys. **37**, 511–520 (1962)
10. H. Lihui, L. Xingren, X. Wu, C. Baojiu, L. Jiuling, Infrared and visible luminescence properties of Er^{3+} and Yb^{3+} ions codoped $Ca_3Al_2Ge_3O_{12}$ glass under 978 nm diode laser excitation. J. Appl. Phys. **90**(11), 5550–5553 (2001)
11. E.S. Yousef, M.M. Elokr, Y.M. AbouDeif, Optical, elastic properties and DTA of TNZP host tellurite glasses doped with Er $^{3+}$ ions. J. Mol. Struct. **1108**, 257–262 (2016)
12. E.S. Yousef, H.H. Hegazy, S. Almojadah, M. Reben, Absorption spectra and Raman gain coefficient in near-IR region of Er^{3+} ions doped TeO_2 –Nb_2O_5 –Bi_2O_3 –ZnO glasses. Opt. Laser Technol. **74**, 138–144 (2015)
13. S. Mohan, K.S. Thind, D. Singh, L. Gerward, Optical properties of alkali and alkaline-earth lead borate glasses doped with Nd^{3+} Ions. Glass Phys. Chem. **34**(3), 265–273 (2008)
14. S.O. Baki, L.S. Tan, C.S. Kan, H.M. Kamari, A.S.M. Noor, M.A. Mahdi, Structural and optical properties of Er^{3+}-Yb^{3+} co-doped multi-composition TeO_2-ZnO-PbO-TiO_2-Na_2O glass. J. Non Cryst. Solids **362**, 156–161 (2013)
15. S.N. Nazrin, M.K. Halimah, F.D. Muhammad, J.S. Yip, L. Hasnimulyati, M.F. Faznny, I. Zaitizila, The effect of erbium oxide in physical and structural properties of zinc tellurite glass system. J. Non Cryst. Solids **490**, 35–43 (2018)
16. N. Chiodini, A. Paleari, G. Brambilla, E.R. Taylor, Erbium doped nanostructured tin- silicate glass-ceramic composites. Appl. Phys. Lett. **80**, 4449–4451 (2002)
17. D. Jaque, J. Capmany, F. Molero, Z.D. Luo, J.G. Sole, Upconversion luminescence in the Nd3+: YAB self-frequency doubling laser crystal. Opt. Mater. **10**, 211–217 (1998)
18. H. Lin, G. Meredith, S. Jiang, X. Peng, T. Luo, N. Peyghambarian, E. Yue-Bun Pun, Optical transitions and visible upconversion

in Er^{3+}-doped niobic tellurite glass. J. Appl. Phys. **93**, 186–191 (2003)
19. P. Nandi, G. Jose, C. Jayakrishnan, S. Debbarma, K. Chalapathi, K. Alti, A.K. Dharmadhikari, J.A. Dharmadhikari, D. Mathur, Femtosecond laser written channel waveguides in tellurite glass. Opt. Exp. **14**, 12145–12150 (2006)
20. A. Amarnath Reddy, S. Surendra Babu, G. Vijaya Prakash, Er^{3+}-doped phosphate glasses with improved gain characteristics for broadband optical amplifiers. Opt. Comm. **285**, 5364–5367 (2012)
21. H. Berthou, C.K. Jorgensen, Optical fiber temperature sensor based on upconversion-excited fluorescence. Opt. Lett. **15**, 1100 (1990)
22. J.F. Phillipps, T. Topfer, H. Ebendorff-Heidepriem, D. Ehrt, R. Sauerbrey, Spectroscopic and lasing properties of Er^{3+}: Yb^{3+}-doped fluoride phosphate glasses. Appl. Phys. B **72**, 399–405 (2001)
23. P. Haro-Gonzalez, I.R. Martin, L.L. Martin, S.F. Leon-Luis, C. Perez-Rodriguez, V. Lavin, Characterization of Er3+ and Nd3+ doped strontium barium niobate glass ceramic as temperature sensors. Opt. Mater. **33**, 742–745 (2011)
24. J.A. Hutchinson, T.H. Allik, Diode array pumped Er, Yb: phosphate glass laser. Appl. Phys. Lett. **60**, 1424–1426 (1992)
25. H. Lin, E.Y.B. Pun, X.R. Liu, Er_{3+}-doped $Na_2O{\cdot}Cd_3Al_2Si_3O_{12}$ glass for infrared and upconversion applications. J. Non Cryst. Solids **283**(1–3), 27–33 (2001)
26. H. Wilke, Organische oberflächenemittierende Laser mit vertikaler Kavität ., PhD, Institute of Nanostructure Technologies and Analytics (INA), Kassel, Germany, (2019)
27. N. Effendy, Z.A. Wahab, S. Abdul Aziz, K.A. Matori, M.H.M. Zaid, S.S.A. Rashid, Characterization and optical properties of erbium oxide doped ZnO–SLS glass for potential optical and optoelectronic materials. Mater. Express **7**(1), 59–65 (2017)
28. E.M.A. Khalil, F.H. Elbatal, Y.M. Hamdy, H.M. Zidan, M.S. Aziz, A.M. Abdelghany, Infrared absorption spectra of transition metals-doped soda lime silica glasses. Phys B **405**(5), 1294–1300 (2010)
29. J. Wong, C.A. Angell, *Glass Structure by Spectroscopy* (Marcel Dekker, New York, 1976)
30. K.H.S. Shaaban, Y. Saddeek, K. Aly, Physical properties of pseudo quaternary $Na_2B_4O_7$ –SiO_2 –MoO_3 –Dy_2O_3 glasses. Ceram. Int. **44**, 3862–3867 (2018)
31. A.A. El-Maaref, K.H.S. Shaaban, M. Abdelawwad, Y.B. Saddeek, Optical characterizations and Judd-Ofelt analysis of Dy^{3+} doped borosilicate glasses. Opt. Mater. **72**, 169–176 (2017)
32. K.S. Shaaban, W.M. Abd-Allah, Y.B. Saddeek, Opt. Quant. Electron **52**, 3 (2020). https://doi.org/10.1007/s11082-019-2094-3
33. H. Darwish, S. Ibrahim, M.M. Gomaa, Electrical and physical properties of Na_2O–CaO–MgO–SiO_2 glass doped with NdF3. J. Mater. Sci. **24**(3), 1028–1036 (2012)
34. T.G.V.M. Rao, A. Rupesh Kumar, C. Kalyan Chakravarthi, M. Rami Reddy, N. Veeraiah, Spectroscopical splitting of Cu ion energy levels in magnesium lead fluoro silicate glasses. Phys B **407**(4), 593–597 (2012)
35. A.M. Efimov, Vibrational spectra, related properties, and structure of inorganic glasses. J. Non-Cryst. Solids **253**(1–3), 95–118 (1999)
36. K.S. Shaaban, Y.B. Saddeek, Effect of MoO_3 Content on structural, thermal, mechanical and optical properties of (B_2O_3-SiO_2-Bi_2O_3-Na_2O-Fe_2O_3) glass system. Silicon **9**(5), 785–793 (2017)
37. M. Imaoka, H. Hasegawa, I. Yasui, X-ray diffraction analysis on the structure of the glasses in the system PbO-SiO_2. J. Non-Cryst. Solids **85**(3), 393–412 (1986)
38. H. Dunken, R.H. Doremus, Short time reactions of a Na_2O-CaO-SiO_2 glass with water and salt solutions. J. Non-Cryst. Solids **92**(1), 61–72 (1987)
39. E.M.A. Khalil, F.H. El-Batal, Y.M. Hamdy, H.M. Zidan, M.S. Aziz, A.M. Abdelghany, UV-visible and IR spectroscopic studies of gamma irradiated transition metal doped lead silicate glasses. Silicon **2**(1), 49–60 (2010)
40. G. Navarra, I. Iliopoulos, V. Militello, S.G. Rotolo, M. Leone, OH-related infrared absorption bands in oxide glasses. J. Non-Cryst. Solids **351**(21–23), 1796–1800 (2005)
41. G. Navarra, R. Boscaino, M. Leone, B. Boizot, Irradiation effects on the OH-related infrared absorption band in synthetic wet silica. J. Non-Cryst. Solids **353**(5–7), 555–558 (2007)
42. K.S. Shaaban, A.A. El-Maaref, M. Abdelawwad, Y.B. Saddeek, H. Wilke, H. Hillmer, Spectroscopic properties and Judd-Ofelt analysis of Dy^{3+} ions in molybdenum borosilicate glasses. J. Lumin. **196**, 477–484 (2018)
43. J.R. Ferraro, M.H. Manghnani, Infrared absorption spectra of sodium silicate glasses at high pressures. J. Appl. Phys. **43**(11), 4595–4599 (1972)
44. M.T. Wang, J.Z. Cheng, M. Li, F. He, Structure and properties of soda lime silicate glass doped with rare earth. Phys B **406**, 187–191 (2011)
45. M.N. Azlan, M.K. Halimah, A.B. Suriani, Y. Azlina, R. El-Mallawany, Electronic polarizability and third-order nonlinearity of Nd^{3+} doped borotellurite glass for potential optical fiber. Mater. Chem. Phys. (2019). https://doi.org/10.1016/j.matchemphys.2019.12181
46. V. Dimitrov, S. Sakka, Electronic oxide polarizability and optical basicity of simple oxides. I. J. Appl. Phys. **79**(3), 1736–1740 (1996)
47. V. Dimitrov, T. Komatsu, Classification of simple oxides: a polarizability approach. J. Solid-State Chem. **163**(1), 100–112 (2002)
48. L. Singh, V. Thakur, R. Punia, R.S. Kundu, A. Singh, Structural and optical properties of barium titanate modified bismuth borate glasses. Solid State Sci **37**, 64–71 (2014)
49. F. El-Diasty, F.A. Abdel Wahab, M. Abdel-Baki, Optical band gap studies on lithium aluminum silicate glasses doped with Cr^{3+} ions. J. Appl. Phys. **100**(9), 093511 (2006)
50. D. Sushama, P. Predeep, Thermal and optical studies of rare earth doped tungsten–tellurite glasses. Int. J. Appl. Phys. Math. **4**, 139–143 (2014)
51. J. Tauc, Electronic properties of amorphous materials. Science **158**, 1543–1548 (1967)
52. E.A.A. Wahab, K.S. Shaaban, Effects of SnO_2 on spectroscopic properties of borosilicate glasses before and after plasma treatment and its mechanical properties. Mater. Res. Express **5**(2), 025207 (2018)
53. A.M. Emara, E.S. Yousef, Structural and optical properties of phosphate-zinc-nickel oxide glasses for narrow band pass absorption filters. J. Mod. Opt. **65**(15), 1839–1845 (2018)
54. S. Thakur, V. Thakur, A. Kaur, L. Singh, Structural, optical and thermal properties of nickel doped bismuth borate glasses. J. Non-Cryst. Solids **512**, 60 (2019)
55. T.Q. Khanh, P. Bodrogi, Q.T. Vinh, *Color Quality of Semiconductor and Conventional Light Sources* (Wiley-VCH, Weinheim, 2017)
56. N. Kaur, A. Khanna, M. Gónzález-Barriuso, F. González, B. Chen, J. Non-Cryst. Solids **429**, 153 (2015)
57. N. Elkhoshkhany, R. Abbas, R. El-Mallawany, S.F. Hathot, Optical properties and crystallization of bismuth boro-tellurite glasses. J. Non-Cryst. Solids **476**, 15–24 (2017)
58. M. Farouk, A. Samir, F. Metawe, M. Elokr, Optical absorption and structural studies of bismuth borate glasses containing Er^{3+} ions. J. Non-Cryst. Solids **371–372**, 14–21 (2013)
59. N. Elkhoshkhany, R. Abbas, R. El-Mallawany, A.J. Fraih, Optical properties of quaternary TeO_2–ZnO–Nb_2O_5–Gd_2O_3 glasses. Ceram. Int. **40**(9), 14477–14481 (2014)

60. Swapna K., Mahamuda SK., Venkateswarlu M., Srinivasa Rao A., Jayasimhadri M., Suman Shakya, Vijaya Prakash G. (2015) Visible, up-conversion and NIR (1.5 μm) luminescence studies of Er^{3+} doped zinc alumino bismuth borate glasses. J. Lumin. **163**, 55–63.
61. T. L. Cottrell, *The Strengths of Chemical Bonds*, 2d ed., (Butterworth, London, 1958) B. deB.
62. Y. Fang, Hu Lili, L. Wen, M. Liao, Judd-Ofelt intensity parameters of Er^{3+} doped mixed alkali aluminophosphate glasses. J. Alloys Compd. **431**, 246–249 (2007)
63. G.N. Hemantha, Kumar, J.L. Rao, K. Ravindra Prasad, Y. C. Ratnakaram, J. Alloys Compd. **480**, 208–215, (2009)
64. Y.C. Ratnakaram, N. V. Srihari, A. Kumar Vijaya, D. Thirupathi Naidu, R.P.S. Chakradhar, Optical absorption and photoluminescence properties of Nd^{3+} doped mixed alkali phosphate glasses-spectroscopic investigations, Spectrochim. Acta Part A **72**, 171–177, (2009)